18TH WORLD CONFERENCE ON EARTHQUAKE ENGINEERING
WCEE2024
MILAN

MILAN, ITALY
30TH JUNE - 5TH JULY 2024

www.wcee2024.it

EXPERIMENTAL CHARACTERIZATION OF INFILL WALLS RETROFITTED WITH NOVEL HOLISTIC TECHNIQUES

A. Furtado[1], H. Rodrigues[2], A. Arêde[3] and H. Varum[3]

CERIS, Instituto Superior Técnico, Lisboa, Portugal, andre.furtado@tecnico.ulisboa.pt

[2] RISCO, Universidade de Aveiro, Aveiro, Portugal

[3] CONSTRUCT, Faculdade de Engenharia da Universidade do Porto, Porto, Portugal

Abstract: *The renovation and refurbishment of existing reinforced concrete (RC) buildings typically focus on enhancing either the structural or thermal energy characteristics of their envelopes. However, growing global concerns regarding the sustainability and resilience of these structures necessitate the development of retrofitting techniques that address both aspects simultaneously. This study aims to validate the effectiveness of novel seismic plus energy retrofitting techniques through a comprehensive testing campaign. To achieve this objective, three full-scale specimens were constructed for experimentation. These three specimens were retrofitted using seismic plus energy retrofitting techniques. Pure out-of-plane (OOP) quasi-static loadings were applied until collapse or partial collapse. The efficiency of each retrofitting solution was assessed by comparing the results of the retrofitted walls with the reference specimen. The findings revealed that the novel combined retrofitting approach significantly improved the thermal transmittance energy efficiency of the walls by approximately 70%. Furthermore, the retrofitting techniques demonstrated notable enhancements in strength and deformation capacity, with improvements of up to 125% and 340%, respectively, compared to the non-retrofitted reference specimen. These results underscore the potential of seismic plus energy retrofitting techniques to achieve dual benefits in terms of energy efficiency and seismic safety. By simultaneously addressing both aspects, these techniques offer a promising avenue for upgrading existing building envelopes. This research contributes to the ongoing efforts to develop sustainable and resilient building practices, aligning with the international imperative to mitigate environmental impacts and enhance the performance of existing structures.*

1 Introduction

The construction sector in the European Union (EU) accounts for 36% of carbon dioxide (CO2) emissions, 40% of energy consumption, and 55% of electricity consumption (Comission 2020). A significant portion of this energy consumption and CO2 emission stems from the heating and cooling of buildings. This trend can be attributed to the delayed introduction of the EU's initial energy codes for buildings, which were only formally established in the 1970s. By that time, approximately 66% of the EU's existing building stock had already been constructed (Bournas 2018). Addressing energy consumption in the building sector is pivotal to meeting the United Nations' goal of achieving net-zero greenhouse gas emissions by 2050. Presently, policies are growing that aim to sustainably renovate existing building structures, primarily focusing on reducing operational energy consumption and incorporating low-carbon materials during refurbishment. However, these policies often overlook structural vulnerabilities, potentially leaving buildings at risk, especially in seismic-sensitive areas.

Structural retrofitting and rehabilitation are typically performed independently from the energy retrofitting interventions (and vice-versa), which can be changed by the implementation of new policies that promote integrated interventions (Masi, Chiauzzi et al. 2019). Furthermore, it is important to note that 40% of these structures are located in earthquake-prone areas and were originally built without sufficient safety measures. Approximately 65% of them are in need of both energy efficiency improvements and seismic retrofitting. Several research works were performed on the validation of independent seismic retrofitting techniques (Kariou, Triantafyllou et al. 2018, De Risi, Furtado et al. 2022) and energy retrofitting (Barreira and de Freitas 2014), but the validation of integrated techniques is still scarce (Pohoryles, Bournas et al. 2022).

Based on this motivation, the present work aims to validate three novel integrated seismic plus energy (SpE) retrofitting techniques for the envelopes of existing Reinforced Concrete (RC) buildings. The techniques aim to reduce the seismic vulnerability of the masonry infill walls against the out-of-plane (OOP) seismic loadings and, at the same time, improve their energy efficiency. Full-scale OOP tests will be performed in three infilled RC frames specimen, with the main goal applying a distributed loading over the walls until reaching their collapse. The results from the retrofitted specimens will be compared with the result from a non-retrofitted wall to better assess the efficiency of the techniques. Along this paper it will be described the testing campaign, retrofitting details of each specimen, test setup and loading protocol. The results will be discussed in terms of damages observed, force-displacement curves, maximum strength capacity and thermal transmittance.

2 Testing campaign

2.1 Objectives and specimens' description

Two main objectives were defined for this testing campaign: i) evaluate the OOP seismic behaviour of masonry infill walls with SpE retrofitting; ii) perform a combined SpE assessment of for each retrofitting technique. To accomplish these objectives three full-scale OOP tests were performed in masonry infill walls (inside RC frames) with combined SpE retrofitting (specimens ES1, ES2 and ES3). The specimen ES1 was retrofitted with a reinforced external thermal insulation composite (ETIC) system technique (i.e., a combination of textile-reinforced mortar, TRM, and ETIC system). The specimen ES2 was retrofitted with a technique comprised by a sequence intervention of TRM and ETIC system. Finally, ES3 was retrofitted with a reinforced thermal plaster. Details of each retrofitting technique will be given in subsection 2.2. The results of these tests will be compared with the result of specimen Inf_08 described in (Furtado, Rodrigues et al. 2022). This specimen has the same geometry, materials and labour as those studied here. The main difference is that the wall was not retrofitted and has only plaster on its external surface. Details concerning the material and mechanical properties of this specimen, herein designated as "REF", can be found in [20].

Regarding the characteristics of the specimens under study, the geometric dimensions of each masonry infill wall are 4.2m in length and 2.30 in height. A general view of the wall before retrofitting is presented in Figure 1a. All the infill panels have equal geometry with the above-mentioned in-elevation dimensions, made of hollow clay horizontal brick units with 150mm thickness. No reinforcement was used to connect the infill panel and the surrounding RC frame since it represents a common construction practice in Southern European Countries. Also, no gaps were used between the panels and the frame elements and no openings. The walls were built aligned with the outer side of the RC beam, as shown in Figure 1b.

a)

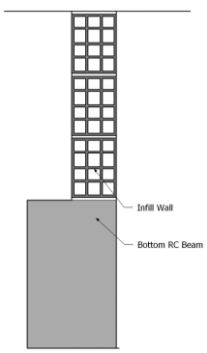

b)

Figure 1. Infilled RC frame without retrofitting: a) general view before retrofitting; and b) profile view.

Each masonry infill wall was built inside an RC frame, composed of RC columns with a cross-section of 300x300mm2 and a longitudinal reinforcement consisting of 4ϕ16+2ϕ12. The transversal reinforcement is ϕ8mm//50mm along the plastic hinge length (500mm) and ϕ8mm//150mm between the plastic hinges. The RC beams have a cross-section of 500x300mm2 and a longitudinal reinforcement consisting of 5ϕ16+5ϕ16. The transversal reinforcement is ϕ8mm//100mm along the plastic hinge length (500mm) and ϕ8mm//200mm between the plastic hinges. The RC frame was designed according to Eurocode 8 for a medium ductility class.

2.2 Retrofitting solutions

Specimen ES1

The retrofit process for specimen ES1 started by securing a 8cm thick EPS plate to the RC frame elements in staggered rows with an adhesive layer, ensuring a 150mm overlap over the RC elements. Subsequently, a new layer of adhesive mortar, approximately 5mm thick, was applied over the external surface of the EPS plate. Next, the Glass-Fibre Reinforced Polymer (GFRP) mesh, assuming the same disposition adopted in the following study (Furtado, Rodrigues et al. 2021) (i.e., overlapping frame-wall, with mesh stripes). The main goal was to reinforce the wall-frame interface. The GFRP mesh was fixed to the wall and to the RC elements using connectors constructed of plastic bushings with steel screws, as illustrated in Figure 2b. These connectors were spaced at 500mm intervals in both horizontal and vertical alignments. To further enhance the structural integrity and prevent cracking, a fresh layer of adhesive plaster was applied to the wall surface, creating a base for the nonstructural mesh. The retrofitting process was completed with the application of approximately 10mm of adhesive plaster.

a) b)

Figure 2. Retrofitting process of specimen ES1: a) general view of application of GFRP mesh over the EPS plates; and b) detailed view of the connectors used.

The GFRP mesh has a tensile strength equal to 40kN/m, an ultimate strain of 3.4% and a grid equal to 16.7x16.7mm^2. No mechanical tests were performed to the nonstructural mesh used.

Specimen ES2

A distinct approach was taken for the retrofit of specimen ES2, involving notable differences in the utilization of fiber-reinforced mortar, connector types, and the placement of a GFRP mesh. The technique used in this specimen was sequence of two interventions, namely first a TRM and second the ETIC system. The retrofit process initiated with the application of 10-20mm of fiber-reinforced plaster in a one-meter-wide strip. This application facilitated the subsequent attachment of the GFRP mesh (same used in ES1), ensuring enhanced adhesion. The GFRP mesh was then positioned over the fresh plaster in a one-meter-wide stripe, with a 150mm overlap onto the RC elements. A 100mm overlap was maintained between adjacent textile meshes.

Once the fiber-reinforced plaster and textile mesh were uniformly applied across the entire panel surface connectors were used to fix the retrofitting mesh. Steel helicoidal connectors were employed. These connectors were exclusively positioned along the interface between the panel and the RC frame elements. The installation process involved pre-drilling the RC frame with an 8mm diameter, followed by punching and bending each connector to ensure a flush fit against the wall face. These connectors were spaced at 500mm intervals and applied along the entire perimeter of the masonry wall. The length of each connector was 500mm and they were only applied in the interface between the frame elements and the wall. The distance between

connector was defined to be 500mm. First, the hole was drilled for each connector and then pushed in the hole with a hammer-vibration-based equipment. The impact of the equipment in the connector ensured that the connector was well fixed. After that, the connector was folded and directed to the wall interior until it touched the mesh. Figure 3a shows the application of these connectors.

After this critical step, 15 days interval were adopted to continue with the application of a ETIC system over the existing TRM retrofitting material. In this case, EPS plates were affixed using adhesive mortar. Subsequently, plastic connectors were introduced, at a rate of 4 per square meter, to secure all the EPS plates to both the wall and frame elements. The final touch involved the application of nonstructural mesh using a thin layer of adhesive mortar, approximately 0.5mm thick. Figure 3b presents the final application of the ETIC system over the TRM material.

a) b)

Figure 3. Retrofitting process of specimen ES2: a) general view of application of helicoidal connectors; and b) application of ETIC system over the TRM material.

Specimen ES3

The retrofitting of specimen ES3 was carried out using a Reinforced Thermal Insulation Mortar technique. The retrofit process initiated with the application of an initial layer of plaster, approximately 10mm thick, designed to enhance bonding properties. Subsequently, a GFRP mesh boasting a tensile strength of 921MPa and a matrix measuring 30x40mm^2 was applied. Connectors were strategically positioned to secure the mesh to both the wall and RC elements. The connectors chosen for this specimen were crafted from a combination of plastic bushings and steel screws, identical to those employed in ES1. These connectors were evenly spaced, maintaining a 500mm interval in both horizontal and vertical dimensions. The next step involved the application of thermal insulation plaster across the entire panel and frame elements, culminating in a total thickness of approximately 70mm, as represented in Figure 4. Following the plaster application, the nonstructural mesh was introduced, and a final layer of plaster, with a thickness ranging from 5 to 10mm, was added to complete the retrofitting system.

Figure 4. Retrofitting process of specimen ES3.

2.3 Test setup, instrumentation and loading protocol

In each quasi-static OOP test, a distributed OOP load was applied across the entire surface of the infill panel through twenty-eight pneumatic actuators. Each actuator was equipped with a wooden plate measuring 500x500mm^2, positioned at the front. To ensure even load distribution and prevent stress concentration or local failures, a 7mm thick cork plate was inserted between the infill wall's surface and the wooden panel. These pneumatic actuators were connected to a robust steel reaction structure, consisting of four horizontal HEB200 steel shapes interacting with five vertical HEB 220 alignments.

The steel reaction structure was anchored to the RC frame at twelve distinct points, comprising five attachment points on the bottom beam, five on the top beam, and two on the middle-height columns. These attachment points utilized steel bars with a diameter of ϕ16mm, which were linked to load cells for real-time monitoring of the OOP loadings. The determination of the number of anchorages was based on numerical simulations, ensuring a well-distributed stress along the RC elements and preventing excessive deflections that could impact the behavior of the masonry infill walls under OOP loads. The primary goal was to establish a self-equilibrated system that effectively balanced the transmission of OOP loads to the reaction frame. More details concerning this test setup can be find in (Furtado, Rodrigues et al. 2021).

In each test, the instrumentation was organized into three distinct groups: i) A total of twenty-five Linear Variable Displacement Transducers (LVDTs) were deployed to assess the OOP displacements of the panel. These LVDTs were strategically placed along five horizontal and vertical alignments, providing comprehensive data on panel movement; ii) An additional set of five LVDTs was employed to gauge the OOP displacement of the RC frame elements, allowing for precise measurement of their response to the applied loads, and iii) A single LVDT was installed in the top beam to monitor the vertical displacements at mid-span. This LVDT played a crucial role in tracking the development of potential arching mechanisms, providing valuable insights into the structural behavior.

Finally, the loading protocol consists of the application of several half-cyclic OOP displacements (loading-unloading-reloading) that were imposed with steadily increasing displacement levels, targeting the following nominal peak displacements at the control node located in the center of the panel: 0.5, 1, 1.5, 2, 2.5, 3.5; 5; 7.5; 10 mm; and then 5 by 5 mm up to a maximum OOP displacement of 120 mm (largest capacity of the pneumatic actuators). Each test stopped when the wall reached the collapse, except for specimen ES2 where it reached only the partial collapse of the wall. Two half-cycles were repeated for each lateral deformation demand level. No axial load was applied at the top of the adjacent RC columns.

3 Results and discussion

The results from the tests will be herein presented first in individual terms, by analyzing the damages observed, and the force-displacement curves of each specimen. After that, global discussion and comparison will be performed by comparing the specimens force-displacement curves (with the reference wall REF), wall thermal transmittance and maximum strength capacity.

3.1 Wall by wall results

Specimen ES1

The test of specimen ES1 revealed three distinct stages of damage. Initially, there was a gradual increase in deformation observed in the central zone of the wall. Subsequently, the lower interface of the wall experienced detachment due to the rupture of plastic connectors. Some bricks were crushed at the bottom zone of the wall resulting from the intense pressure near the bottom interface. The deformation between connectors at the bottom interface continued to escalate until each connector ultimately failed. Following the failure of all connectors located in the bottom RC beam, there was a significant increase in deformation in this area. Next, the failure of the first connector positioned at mid-span in the upper RC beam was observed. This phenomenon then repeated for the remaining connectors in the upper RC beam. At this point, the wall relied solely on the connectors of the RC columns, causing an increase in deformation in the central zone, mimicking the behavior of a panel subjected to unidirectional bending, akin to a simply supported beam. Finally, the wall's collapse ensued as a result of the failure of the connectors affixed to the RC columns, transforming the panel into a rigid body. The moment of collapse mechanism is shown in Figure 5a.

The force-displacement curve, detailed in Figure 5b, revealed an initial stiffness of 13.66kN/mm and a peak load of 81.35kN at an OOP drift of 1.98%. Conventional failure occurred when the OOP drift reached 3.89%. The ultimate collapse transpired at an OOP drift of 11.48% with a corresponding force of 16.54kN.

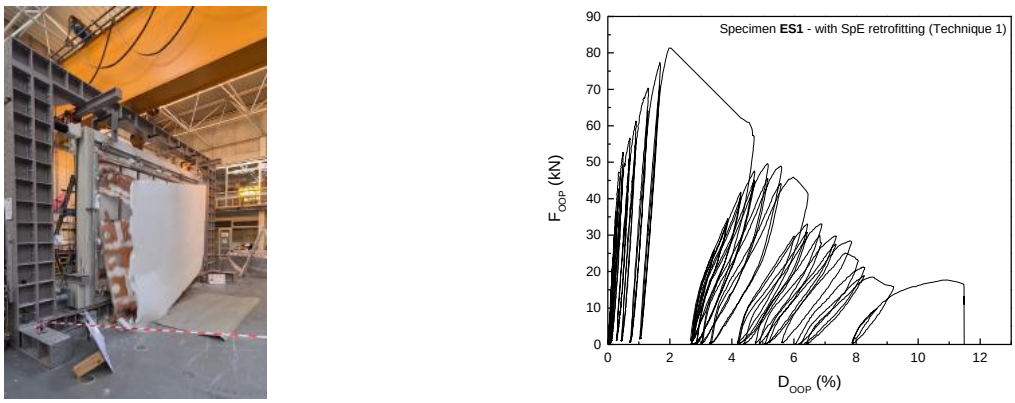

a) b)

Figure 5. Results of specimen ES1: a) failure mode during the collapse; and b) force-displacement curve.

Specimen ES2

The detachment of the wall initiated at the top interface, visible in Figure 6a, under relatively low displacement demands, approximately 3mm. This detachment gradually increased in thickness, exceeding 20mm. At this point, there was a noticeable collapse of the bricks on the inner face of the wall (i.e., the side facing the pneumatic actuators). Simultaneously, there was a slight detachment of the wall at the bottom interface until the connectors positioned in the upper RC beam experienced rupture. Subsequently, the wall transformed into a rigid body, with support primarily on the bottom RC beam. The remaining connectors within the RC elements prevented the wall's complete collapse up to this stage. After reaching significant deformation, the wall underwent a partial collapse characterized by three key features: i) division of the wall into two half-span sections; ii) complete separation of the wall from the top RC beam; and iii) partial support remaining along the side edges and the bottom RC beam. The remarkable efficiency of the connectors used in this strengthening solution was evident, as they effectively prevented the wall's collapse even when subjected to high drift values.

In Figure 6b, the force-displacement curve is presented, revealing an initial stiffness of 31.89kN/mm and a peak load of 99.17kN at an Out-of-Plane (OOP) drift of 3.19%. After reaching the peak load, the detachment of the wall at the top interface led to a reduction in the panel's strength. Conventional failure transpired at an OOP drift of 7.48%. As previously mentioned, the complete collapse of the wall did not occur; instead, the test was halted at an OOP drift of 14.74%.

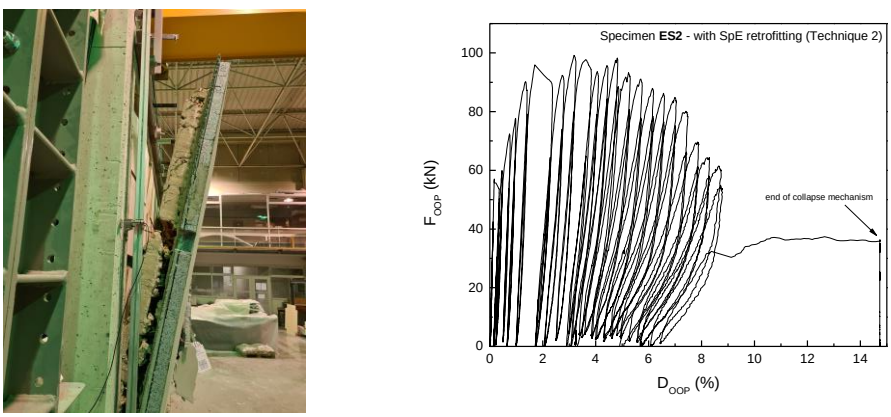

a) b)

Figure 6. Results of specimen ES2: a) view of the partial collapse; and b) force-displacement curve.

Specimen ES3

During the first cycle, an accumulation of the OOP deformation primarily concentrated in the central region of the wall, along with the initial appearance of cracks in the thermal plaster. These cracks were limited to the left and right sides of the wall, as the cracking mesh on the external face of the composite retrofitting system effectively prevented further propagation. The comparatively lower tensile strength of the thermal plaster rendered it more prone to cracking, especially when compared to stronger materials like fiber-reinforced plasters. The observed cracking continued to grow in thickness until the wall ultimately detached at the top interface. This detachment became increasingly pronounced as the test progressed, culminating in the collapse of the wall, shown in Figure 7a. The collapse occurred without any visible significant structural damage or preceding reduction in strength as can be seen in the force-displacement curve plotted in Figure 7b. The wall's collapse was attributed to the connectors positioned at the end (edge) of the reinforcing, which could not prevent local mesh failure and the detachment of the retrofitting composite material. Filaments at the ends of the mesh were inherently more fragile and prone to breakage. This fragility was exacerbated by the fact that the frame net had larger grid dimensions compared to the net used in walls ES_1 and ES_2, which diminished the efficiency of the anchorage. Consequently, the mesh failed at the ends around the connectors affixed to the RC elements, leaving the wall without any element anchoring it to the frame. The collapse mechanism initiated once a substantial detachment occurred at the top interface. The factors contributing to the fragile wall's collapse at low displacement demands were identified as follows: i) the absence of overlapping of the mesh along the interface between the wall and frame elements; ii) mesh rupture near the connectors located in the RC frame elements; iii) the larger mesh matrix dimensions, leading to a higher likelihood of generating extremely high stresses in the mesh strands when they came into contact with the connectors.

From the analysis of the force-displacement curve, illustrated in Figure 7b, it can be extracted an initial stiffness of 18.54kN/mm and a peak load of 66.91kN at an OOP drift of 3.16%. Conventional failure did not occur before the initiation of the collapse mechanism, which commenced at an OOP drift of 4.11%.

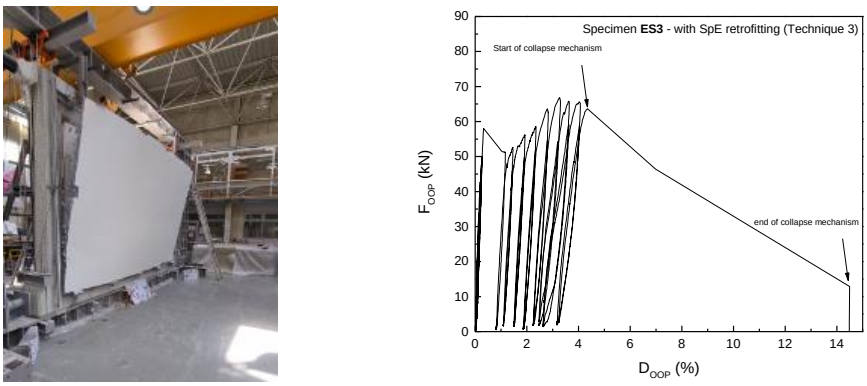

a) b)

Figure 7. Results of specimen ES3: a) view of the collapse mechanism; and b) force-displacement curve.

3.2 Global results

Figure 8 presents the comparison of the force-displacement curves of the retrofitted specimens with the reference specimen. From its analysis the impact of the integrated retrofitting techniques on the maximum peak load is evident when examining the results. Walls retrofitted demonstrated substantial peak loads, with wall ES2 reaching 125% higher than the REF specimen (Figure 8b), ES1 achieving 84% higher (Figure 8a), and ES3 showing a remarkable 52% improvement (Figure 8c). Wall ES3 poor performance can be explained by the inefficiency of its anchorage system in securing the retrofitting material to the frame elements. Regarding the drift at which the peak load was reached, panel ES1 reached it for an OOP drift slightly lower than that observed in the REF (approximately 10%). In contrast, the remaining walls retrofitted with SpE techniques achieved the peak load at OOP drift values 40% higher than REF. Conventional failure (i.e., a 20% drop in strength after the peak load) was observed only in walls ES1, and ES2. The level of drift corresponding to conventional failure varied, occurring at low deformation demands for specimen ES_1 and at higher demands for ES_2. Finally, the collapse occurred in panels REF, ES1, and ES3. Notably, panel ES_1 exhibited the

highest collapse drift, approximately 332% higher than REF, highlighting the vulnerability of non-retrofitted masonry infill walls. Retrofitting technique used in ES2 proved highly effective in preventing wall collapse.

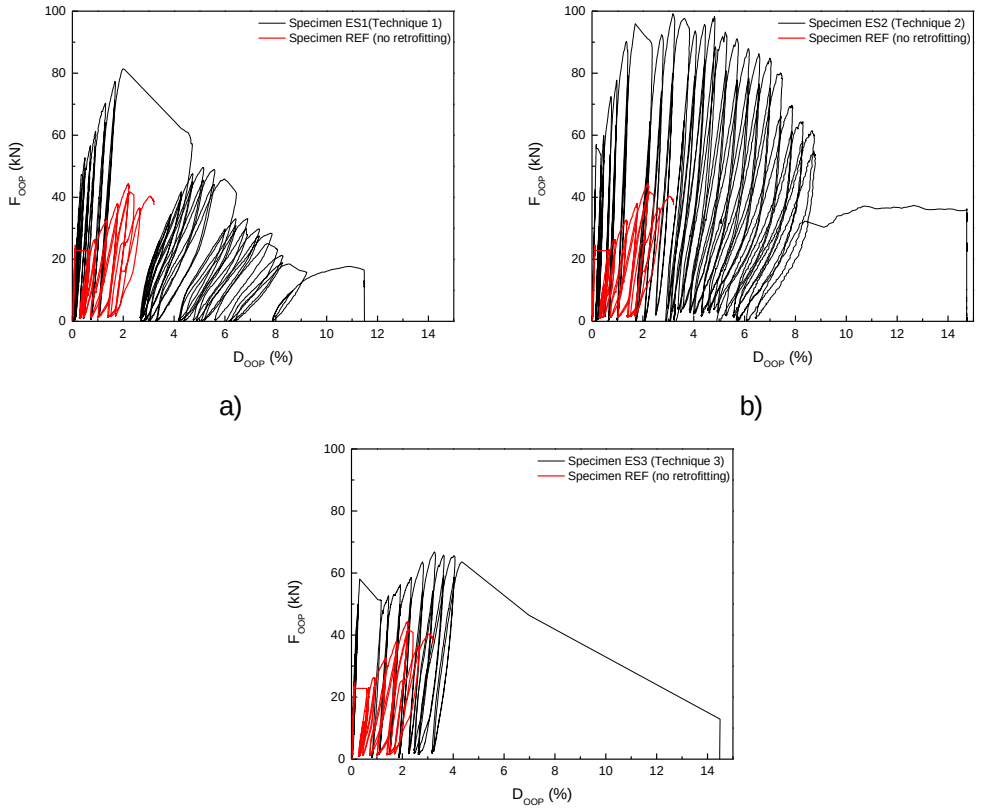

Figure 8. Global results comparison: force-displacement curves a) ES1-REF; b) ES2-REF; and c) ES3-REF.

From the analysis, of the comparison between the maximum strength capacity plotted in Figure 9a it can be observed that the specimen ES2 reached the highest strength with 99.17kN, followed by ES1 and ES3, respectively 81.35kN and 66.91kN. The maximum strength capacity of the REF specimen was 55.90kN.

The thermal transmittance U_{value} was computed for all the walls herein tested using the R_{value} of each layer of the masonry wall (i.e. masonry units, coatings and strengthening material). The U_{value} was computed according to the proposal of EN ISO 6946 (ISO 2017). Each layer's values λ (thermal conductivity coefficient) or U_{value} were necessary for this calculation. In the computing of U_{value}, R_{si} represents the internal surface thermal resistance (value according to EN ISO 6946 (ISO 2017)), R_{se} represents the external surface thermal resistance (value according to EN ISO 6946 (ISO 2017)) and R_j is the thermal resistance of the layer of each material.

The U_{value} was determined to be 1.76, 0.35, 0.30, and 0.37 m^2KW^{-1} for the walls REF, ES1, ES2, and ES3, respectively. The direct comparison of U_{value} for each wall is presented in Figure 9b. It is evident that walls ES1, ES2, and ES3 exhibit significantly lower U_{value} compared to REF. This reduction is attributed to the incorporation of thermal insulation materials. Wall ES2 achieved the lowest U_{value}, approximately 83% lower than that of REF, and about 15% and 19% lower than ES_1 and ES_3, respectively.

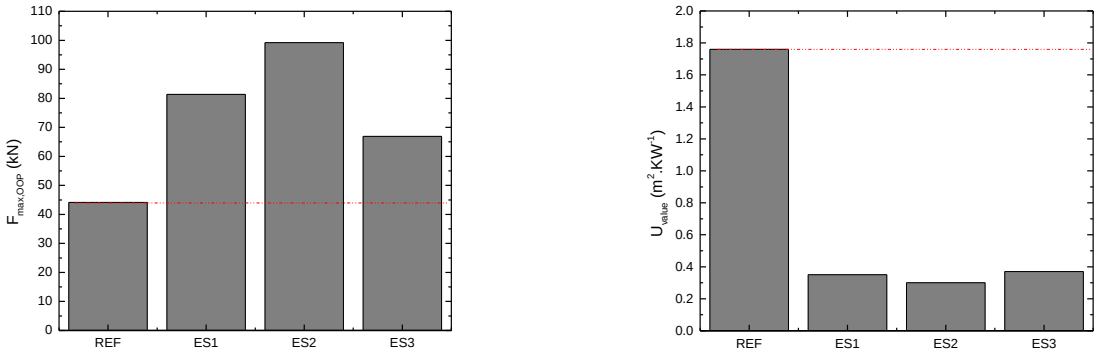

a) b)

Figure 9. Global results comparison: a) Maximum OOP strength; b) Thermal transmittance.

4 Conclusions

The renovation and refurbishment of existing envelopes of RC buildings typically prioritize either structural or thermal energy improvements in isolation. However, given the growing global emphasis on the sustainability and resilience of existing building structures, it has become imperative to reconsider retrofitting techniques that can effectively address both aspects simultaneously. To address this need, a comprehensive testing campaign was conducted to validate the efficiency of innovative integrated retrofitting techniques, in direct comparison to a non-retrofitted configuration.

Three full-scale specimens were constructed for this study, comprising three walls with integrated seismic plus thermal energy retrofitting The following conclusions were drawn from this research: i) The impact of integrated retrofitting on the initial stiffness of the infill walls presented mixed results. In some instances, the initial stiffness was observed to be lower compared to non-retrofitted configurations. Ii) Integrated retrofitting significantly increased the maximum strength of the walls, namely enhanced the peak load by 52% to 125%; iii) Conventional failure was observed exclusively in walls with integrated retrofitting; iv) In terms of deformation capacity, integrated retrofitting demonstrated an efficient performance, with the collapse occurring at large OOP drift values up to 3.32 times higher than the non-retrofitted wall.

Generally, the type of connectors used played a crucial role in retrofitting efficiency. Steel connectors contributed to a substantial increase in wall displacement and strength capacity. Helicoidal connectors were particularly effective in preventing total wall collapse. Walls retrofitted with thermal plaster exhibited energy-saving properties comparable to walls retrofitted with EPS layers and steel connectors.

These conclusions are drawn from a limited number of pure OOP tests and require additional validation, particularly under combined in-plane and OOP loading conditions.

5 Acknowledgments

The first author is grateful for the Foundation for Science and Technology's support through funding UIDB/04625/2020 from the research unit CERIS.This work was also financially supported by: Project POCI-01-0145-FEDER-007457 - CONSTRUCT - Institute of R&D In Structures and Construction funded by FEDER funds through COMPETE2020 - Programa Operacional Competitividade e Internacionalização and by national funds through FCT - Fundação para a Ciência e a Tecnologia. This work was also supported by the Foundation for Science and Technology (FCT) - Aveiro Research Centre for Risks and Sustainability in Construction (RISCO), Universidade de Aveiro, Portugal [FCT/UIDB/ECI/04450/2020].

The authors would like to acknowledge Fassa Bortolo for all the materials supplied and technical support that were fundamental for the development of the testing campaign. The authors would also like to acknowledge the Laboratory of Earthquake and Structural Engineering (LESE) technicians, Mr. Guilherme Nogueira and Mr. Nuno Pinto, for supporting the experimental activity reported in this research work.

6 References

Barreira, E. and V. P. de Freitas (2014). "External Thermal Insulation Composite Systems: Critical Parameters for Surface Hygrothermal Behaviour." Advances in Materials Science and Engineering **2014**: 650752.
Bournas, D. A. (2018). "Concurrent seismic and energy retrofitting of RC and masonry building envelopes using inorganic textile-based composites combined with insulation materials: A new concept." Composites Part B: Engineering **148**: 166-179.
Comission, E. (2020). "A renovation wave for Europe - greening our buildings, creating jobs, improving lives."
De Risi, M. T., A. Furtado, H. Rodrigues, J. Melo, G. M. Verderame, A. Arêde, H. Varum and G. Manfredi (2022). "Influence of textile reinforced mortars strengthening on the in-plane/out-of-plane response of masonry infill walls in RC frames." Engineering Structures **254**: 113887.
Furtado, A., H. Rodrigues, A. Arêde, J. Melo and H. Varum (2021). "The use of textile-reinforced mortar as a strengthening technique for the infill walls out-of-plane behaviour." Composite Structures **255**: 113029.
Furtado, A., H. Rodrigues, A. Arede and H. Varum (2022). "Experimental Investigation on the Possible Effect of Previous Damage, Workmanship and Test Setup on the Out-of-plane Behaviour of Masonry Infill Walls." Journal of Earthquake Engineering **26**(11): 5647-5678.
ISO (2017). "ISO 6946:2017, Building components and building elements — Thermal resistance and thermal transmittance — Calculation methods."
Kariou, F. A., S. P. Triantafyllou, D. A. Bournas and L. N. Koutas (2018). "Out-of-plane response of masonry walls strengthened using textile-mortar system." Construction and Building Materials **165**: 769-781.
Masi, A., L. Chiauzzi, G. Santarsiero, V. Manfredi, S. Biondi, E. Spacone, C. Del Gaudio, P. Ricci, G. Manfredi and G. M. Verderame (2019). "Seismic response of RC buildings during the Mw 6.0 August 24, 2016 Central Italy earthquake: the Amatrice case study." Bulletin of Earthquake Engineering **17**(10): 5631-5654.
Pohoryles, D. A., D. A. Bournas, F. Da Porto, A. Caprino, G. Santarsiero and T. Triantafillou (2022). "Integrated seismic and energy retrofitting of existing buildings: A state-of-the-art review." Journal of Building Engineering **61**.